CRYSTAL GROWTH & DESIGN

Article

pubs.acs.org/crystal

Shape-Controlled Vapor-Transport Growth of Tellurium Nanowires

Christopher J. Hawley, Brian R. Beatty, Guannan Chen, and Jonathan E. Spanier*

Department of Materials Science & Engineering, Drexel University, Philadelphia, Pennsylvania, United States

Supporting Information

ABSTRACT: A vapor transport method is employed to synthesize single crystalline tellurium nanowires with tailorable size using tellurium powder in an inert atmosphere. The average nanowire diameter is tunable between 50 and 3000 nm with an associated length of 1 to 22 μm. Growth temperature and time are used to specifically control the behavior of supersaturation, leading to nucleation and morphological control in this vapor−solid growth regime. Analysis of the resulting nanowire product provides insight into the dominant reaction kinetics involved in these growths and suggests routes by which to control growth product. This methodology provides a practical approach to synthesizing high-quality tellurium nanowires of various sizes and their incorporation into two-dimensional mesh-like structures through controlled nucleation and growth dynamics.

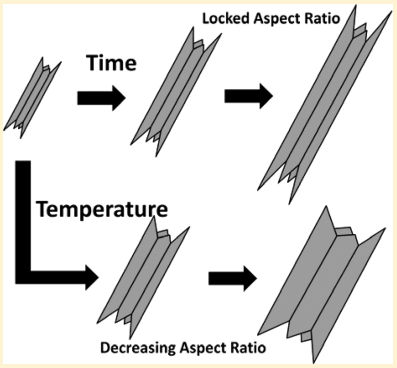

INTRODUCTION

Nanowires and nanostructures continue to attract attention with the promise of potential applications in a variety of fields including electronics, photonics, biomedicine, and catalysis.[1−3] Nanostructures provide an ideal framework with which to investigate carrier confinement and finite size effects on electric, optical, and magnetic systems. Elemental tellurium (Te), a narrow bandgap p-type semiconducting metalloid, has shown great potential for application because of its intrinsically photoconductive and piezoresistive characteristics in addition to its nonlinear optical, thermoelectric, and catalytic properties.[4−11] Furthermore, due to the highly anisotropic crystalline structure of Te, the system favors 1D nanostructured growth. The growth of Te nanostructures, as with the bottom-up field as a whole, has two primary preparations: wet synthesis[12−20] and vapor transport.[21−25] In both disciplines, techniques involving template growth[26] and catalytic growth[27−31] help direct nanostructure growth. Though Te nanostructures have shown to be very rich in different morphologies, quantitative control of nanowire growth product has only been reported using selected wet synthesis techniques[12−14,18,20,32] and is primarily accomplished by flow control of supersaturation. Vapor transport growths are inherently more advantageous in this system due to the controlled orientation of the single crystalline product, which lends itself better to device fabrication. Here, we present the controlled vapor−solid growth of Te nanowires on silicon dioxide with tailorable diameter and length based on deposition vapor temperature as well as deposition time. Variations in the growth parameters control the nanowire growth and their evolution into polycrystalline films. Such morphology control, combined with the ability to transform these tailorable nanostructures into other compounds, provides the framework for future bottom-up device fabrication.

EXPERIMENTAL SECTION

Thermally grown, 200 nm thick silicon dioxide on Si(111) wafers was cleaned with solvents and DI water followed by oxygen plasma cleaning to remove organic residues. Te powder (99.999%, Alfa-Aesar) was placed in an alumina boat upstream of the substrate. In a typical growth, the boat was held at 300 °C for the duration of the growth while the temperature gradient on the substrate extended from 150 to 280 °C. The entire process was performed using a flow of either Ar or H_2 at 25 sccm at a pressure of 1 Torr. Additional two-temperature growths were performed to nucleate and grow a higher density of wires and nanostructures.

Characterization. X-ray diffraction (XRD) spectra were obtained using a Rigaku SmartLab X-ray diffractometer with Cu−K_α radiation (λ = 1.542 Å). The 2θ range used spanned 20° to 80° in steps of 0.05° at a scan rate of 1°/min. The Te postgrowth nanowire morphology was imaged with field-emission scanning electron microscopy (SEM, FEI DB235 and Amray 1850). Selected area electron diffraction (SAED) and energy-dispersive X-ray spectra (EDS) were taken using a JEOL JEM2100 LaB_6 transmission electron microscope (TEM) at a 200 kV accelerating voltage.

RESULTS AND DISCUSSION

The morphology of the as-grown Te nanowires varies from 30 nm to over 6 μm in diameter and from a few hundred nanometers to over 30 μm in length. Shown in Figure 1 is the typical nanowire product of the vapor−solid Te growths. The nanowires have hexagonal cross sections with concave ends, consistent with other vapor and wet growths.[33−35] TEM images and SAED patterns reveal the single crystallinity and typical growth orientation of ⟨001⟩ for the Te nanowires (Figure 2). Compositional purity was confirmed via EDS and affirms that the nanostructures consist of pure elemental Te. The XRD

Received: October 30, 2011
Revised: February 23, 2012
Published: April 17, 2012

dx.doi.org/10.1021/cg2014368 | Cryst. Growth Des. 2012, 12, 2789−2793

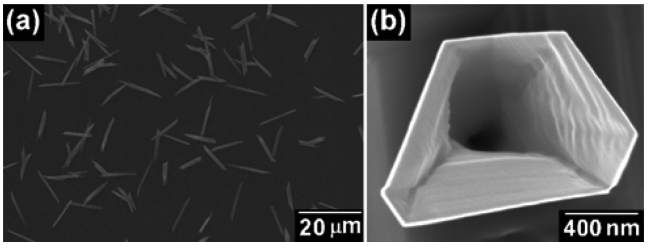

Figure 1. SEM micrograph showing the results typical of vapor−solid growth of Te nanowires (a) and (b) a Te nanowire viewed along the ⟨001⟩ axis demonstrating that the concave morphology does not extend through the nanowire.

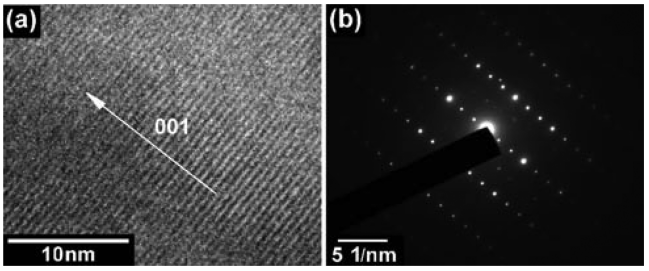

Figure 2. High-resolution TEM of a Te nanowire (a) with associated SAED pattern (b) showing the *c*-axis unit cell periodicity of 0.59 nm.

peaks collected from as-synthesized nanowires on the growth substrate (Figure 3) can be indexed to the pure Te hexagonal

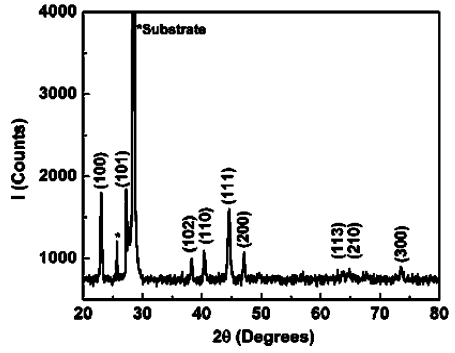

Figure 3. An XRD spectrum with characteristic tellurium peaks. The starred peaks (∗) are due to the silicon/silicon dioxide substrate.

structure of space group $P3_121$ (No. 152) with two additional peaks from the growth substrate.

The experimental setup specifically enhances the supersaturation by utilizing substrates that span extended lengths along the furnace's downstream temperature gradient. The silicon wafer substrates are shown to equilibrate to a median temperature, thus creating an abrupt change in local equilibrium vapor pressure, as seen in Figure 4. In contrast, when similarly prepared shortened substrates are placed side by side with the longer substrates, the smaller substrates are observed to be below the critical supersaturation level because there is no evidence of any nucleation or growth. A supersaturation controlled growth regime is consistent with the lack of nucleation and growth beyond where the ratio of the vapor pressure to the equilibrium vapor pressure at the substrate passes through unity on these long substrates.

The subsequent analysis of the as-grown substrates tells much about the reaction dynamics of the vapor transport

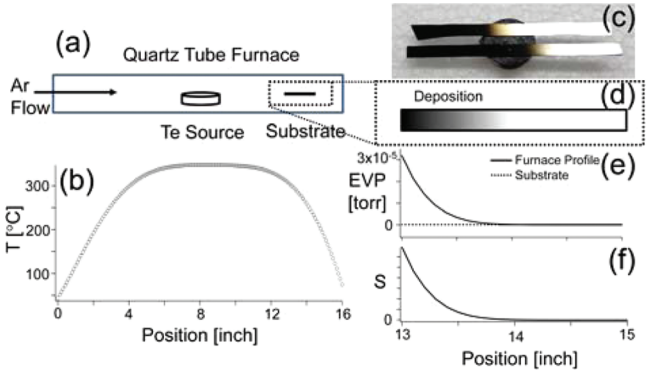

Figure 4. (a, b) The experimental setup and furnace profile of a typical nanowire growth. (c) Two as-grown substrates showing the Te deposition regions (black), which can be modified using carrier flow, pressure, etc. but are mainly dictated by the local equilibrium vapor pressure. (d, e, f) Using the equilibrium vapor pressure of Te associated with a temperature profile of the furnace, which is an underestimate of the vapor pressure as the $Te_2(g)$ is transported from the higher temperature region, we can extrapolate the expected supersaturation behavior along the substrate. This agrees with the deposition profile observed.

growth. We find nonwetted morphologies consistent with the fact that semimetal Te bonds to itself preferentially instead of breaking Si−O surface bonds. Furthermore, a nearly constant nucleation density spans the range of supersaturation along the substrate, $\sim 0.015/\mu m^2$. This is expected for nucleation dominated by active surface sites (steps, defects, impurities, etc.),[36] whereas classical nucleation rates and the concentration of critical nuclei will depend on supersaturation as well as temperature.[37] Active surface sites as the primary means of nucleation are also suggested by the relatively narrow size distribution of the nanowires because the energetically available sites nucleate nanowires quickly at a density determined by the substrate quality. Classical nucleation would continue to nucleate wires, as long as feeding the wire growth does not lead to prohibitively lowering the supersaturation. As is common in nanowire growth, we observe enhanced nucleation of specifically roughened surfaces due to the increase of surface defects. Access to higher nucleation densities can also be achieved by briefly increasing the substrate and source temperature to nucleate seed crystallites at otherwise energetically inaccessible surface sites and then continue growth at a lower temperature.

The growth rate of the Te nanowires is driven not only by the magnitude of supersaturation induced by temperature[38] but also by the surface energy landscape (Figure 5). In the investigation of the as-grown nanowires, a characteristic thermal activation relationship indicative of a rate-limiting surface reaction is evident. Activation energies of 1.17 ± 0.04 eV and 1.07 ± 0.02 eV are measured for nanowire length and diameter growth, respectively, as shown in Figures 6 and 7. This effective activation energy is a composite of many processes, such as diffusion through the boundary layer, physisorption, surface diffusion on SiO_2, as well as Te, etc. We attribute the primary rate-limiting step associated with this energy to be the dissociative chemisorption activation energy that must be overcome for a physisorbed $Te_2(g)$ molecule to become incorporated into the Te nanowire. The higher temperature vapor further upstream possesses greater available energy with which to overcome this activation barrier. Noting that the mean

dx.doi.org/10.1021/cg2014368 | *Cryst. Growth Des.* 2012, 12, 2789−2793

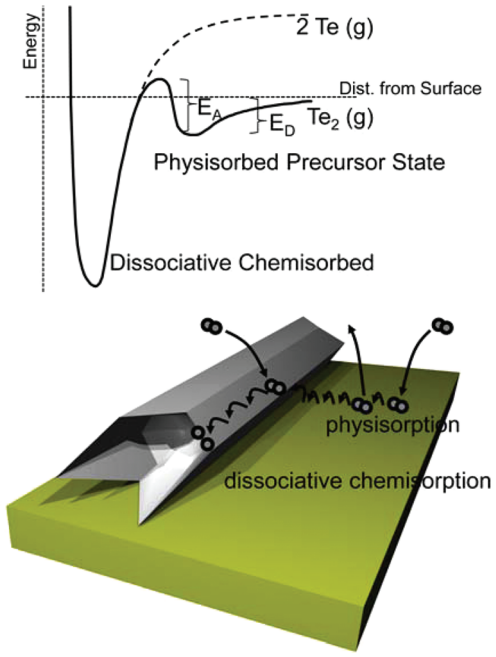

Figure 5. Simple surface chemistry model indicating the adsorption into a precursor state where the Te molecules can diffuse about the surfaces, eventually dissociating to chemisorb into the Te nanowire. Molecules diffusing about the surface demonstrate how the concave nature of these nanowires occurs.

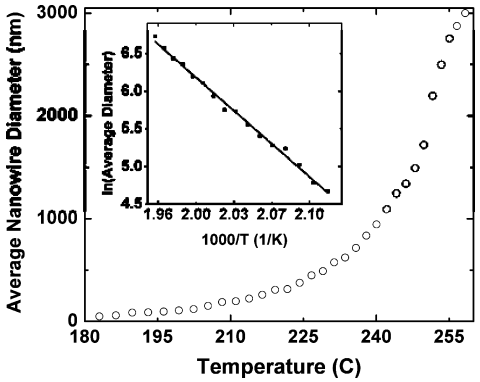

Figure 6. The average nanowire diameter as a function of furnace temperature taken from a single long substrate. The inset demonstrates the thermally activated nature of the relationship of a subset of the data, which excludes the mass-transport at high temperature and the low temperature region where our supersaturation-induced nucleation and growth regime ends.

free path of a Te_2(g) molecule is significantly greater than the nanowire diameter length scale, it is less likely that Te_2(g) molecules will fall incident within the end cavity of a nanowire. The most probable path of Te_2(g) is to first impinge on a nanowire or migrate from the SiO_2 surface and then diffuse via physisorption site to site until a defect or void energetically favorable for crystallographic incorporation is found. Dissociative chemisorption of Te_2(g) will only occur along the *c*-axis of the nanowire in this case if no favorable {100} face site is encountered. This nontrivial contribution from surface diffusion along the {100} faces explains the difference in effective activation energies between diameter and length through variations in the energetic landscapes as well as the highly faceted nature of the {100} faces and the material

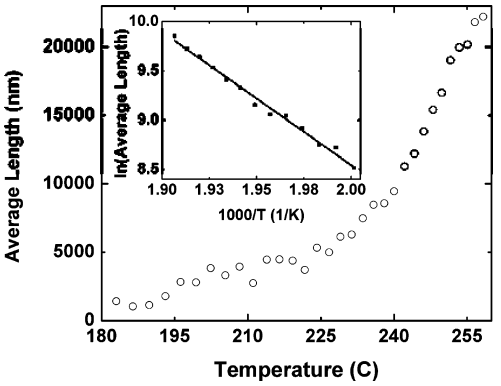

Figure 7. The average nanowire length as a function of furnace temperature along the same substrate as seen in Figure 6. The inset shows a similar thermally activated process that is observed with nanowire diameter.

starved end cavity along the {001} from the diffusing Te_2(g) encountering the strong *c*-axis covalent bonding, leading to lower diffusion in crystallographically anisotropic Te. In our Te growths, we specifically used temperature and supersaturation as a means by which to drive the previously mentioned kinetics, with the expectation that a higher energy Te molecule will lead to higher chemisorption rates for both {100} and {001} face growth, and thus allow for the tailoring of the nanowire morphology (Figure 7). Such behavior is seen on a single substrate spanning a wide range of supersaturation. At a constant temperature, the aspect ratio is not expected to change in time as there is no change in the energetic landscape. Holding the substrate and furnace temperature constant, we find that as a function of growth duration the aspect ratio is relatively constant. Figure 8 indicates this for the profile

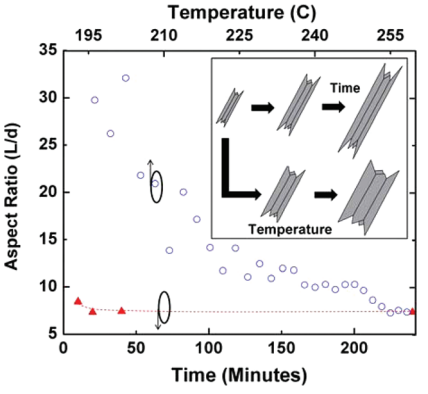

Figure 8. The aspect ratio of the nanowires as a function of time for a single position (260 °C) as well as temperature along a single substrate demonstrating the ability to use each independently to tailor the growth product. Constant aspect ratios were seen at other positions as well. The inset shows the morphological trends resulting from the changes induced in the energetic landscape.

position associated with 260 °C, and a similar behavior is observed for the other furnace positions as well.

As typical with most nanowire growth, we find that the nucleation probability is highly dependent on substrate temperature.[27,39,40] A study of Te growth shows that a high-temperature nucleation step can significantly improve the nanowire nucleation rate, resulting in an enhanced and controlled nanowire density. Following the initial nucleation

dx.doi.org/10.1021/cg2014368 | *Cryst. Growth Des.* 2012, 12, 2789–2793

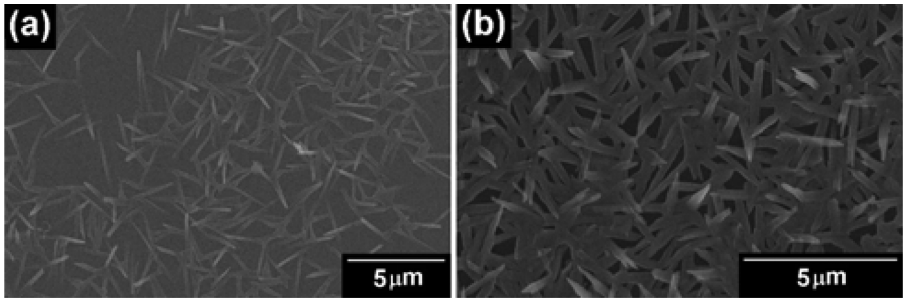

Figure 9. Increased nanowire nucleation as a result of two-step temperature growth producing 2-D tailorable nanowire meshes. Shown are two positions along a substrate utilizing the same experimental setup as in Figure 4. The lower temperature furnace positions produce on average smaller diameter nanowires, 192 nm (a) compared with 303 nm (b). The lower growth rate at reduced temperatures produces a nanostructure with tunable porosity, 0.13 and 0.56 for the low- and high-temperature positions shown here, respectively.

step with a lower temperature growth step cultivates smaller diameter nanowires at high growth density. Utilizing two-step growth, we produced elemental Te nanowire meshes of various nanowire diameters consistent with the previously discussed growth as well as porosities (Figure 9). Because these structures span the growth regime where the nanowires grow into films, the desired porosity and composite nanowire dimension span a smaller positional range on the substrates as further upstream (downstream) nanowires grow at a higher (lower) rate, thus resulting in larger (smaller) length and diameter wires, which also nontrivially affects porosity. In further downstream regions from the desired mesh nanostructures, networks of in-plane nanowires do not have the axial growth rate to connect into networks.

■ CONCLUSION

In summary, we have studied the nucleation and growth of Te nanowires and have developed a means by which to controllably grow 2-D nanowire mesh structures with hexagonal cross sections. Such growth demonstrates control over the nanowire morphology via supersaturation and surface dynamics by sublimation source temperature, substrate temperature, and growth time. Grown via vapor transport method, these nanowire structures are found to be high-purity single-crystalline Te and are shown to preferentially grow along the SiO_2 surface of the substrates at temperatures ranging from 150 to 280 °C. The tailorablility of these Te nanowires and structures is potentially useful for bottom-up fabrication of nanodevices with specific size-dependent properties.

■ ASSOCIATED CONTENT

Supporting Information

Energy-dispersive X-ray spectroscopy of the nanowires taken with the TEM previously mentioned. The EDS shows the purity of the nanowire samples with the primary peaks identified as the characteristic elemental Te peaks and Cu peaks from the TEM grid. This material is available free of charge via the Internet at http://pubs.acs.org.

■ AUTHOR INFORMATION

Corresponding Author

*Author e-mail address: spanier@drexel.edu.

Notes

The authors declare no competing financial interest.

■ ACKNOWLEDGMENTS

We thank Christopher B. Murray of the University of Pennsylvania for discussions and for providing access to the Rigaku SmartLab X-ray diffractometer in his laboratory to carry out some of the structural analysis reported in this work. TEM imaging and analysis was performed in the Drexel Centralized Research Facilities. J.E.S. acknowledges the US Army Research Office for support of this work under W911NF-08-1-0067, and for instrumentation support under NSF DMR 0722845. C.J.H. was supported by an NSF IGERT Fellowship (DGE 0654313) and by a US Dept. of Education GAANN-RETAIN Assistantship (P200A100117), and G.C. was supported on NSF DMR 0907381.

■ REFERENCES

(1) Duan, X.; Huang, Y.; Cui, Y.; Wang, J.; Lieber, C. M. *Nature* **2001**, *409*, 66−69.
(2) Huang, M. H.; Mao, S.; Feick, H.; Yan, H.; Wu, Y.; Kind, H.; Weber, E.; Russo, R.; Yang, P. *Science* **2001**, *292*, 1897−1899.
(3) Lieber, C. M.; Wang, Z. L. *MRS Bull.* **2007**, *32*, 99−108.
(4) Araki, K.; Tanaka, T. *Jpn. J. Appl. Phys.* **1972**, *11*, 472.
(5) Berger, L. I. *Semiconductor Materials*; CRC Press: Boca Raton, FL, 1997.
(6) Cooper, W. C. *Tellurium*; Van Nostrand Reinhold Co.: New York, 1971; p 437.
(7) von Hippel, A. *J. Chem. Phys.* **1948**, *16*, 372−380.
(8) Ufimtsev, V. B.; Osvensky, V. B.; Bublik, V. T.; Sagalova, T. B.; Jouravlev, O. E. *Adv. Perform. Mater.* **1997**, *4*, 189−197.
(9) Weidmann, E. J.; Anderson, J. C. *Thin Solid Films* **1971**, *7*, 265−276.
(10) Kudryavtsev, A. A. *The Chemistry & Technology of Selenium and Tellurium*; Collet's: London, 1974.
(11) Givargizov, E. I. *Highly Anisotropic Crystals*; D. Reidel: Dordrecht, the Netherlands, 1987.
(12) Gautam, U. K.; Rao, C. N. R. *J. Mater. Chem.* **2004**, *14*, 2530−2535.
(13) Liu, Z.; Hu, Z.; Xie, Q.; Yang, B.; Wu, J.; Qian, Y. *J. Mater. Chem.* **2003**, *13*, 159−162.
(14) Mayers, B.; Xia, Y. *J. Mater. Chem.* **2002**, *12*, 1875−1881.
(15) Mo, M.; Zeng, J.; Liu, X.; Yu, W.; Zhang, S.; Qian, Y. *Adv. Mater.* **2002**, *14*, 1658−1662.
(16) Qian, H. S.; Yu, S. H.; Luo, L. B.; Gong, J. Y.; Fei, L. F.; Liu, X. M. *Chem. Mater.* **2006**, *18*, 2102−2108.
(17) Song, J. M.; Lin, Y. Z.; Zhan, Y. J.; Tian, Y. C.; Liu, G.; Yu, S. H. *Cryst. Growth Des.* **2008**, *8*, 1902−1908.
(18) Tang, Z.; Wang, Y.; Sun, K.; Kotov, N. A. *Adv. Mater.* **2005**, *17*, 358−363.
(19) Xi, G.; Peng, Y.; Yu, W.; Qian, Y. *Cryst. Growth Des.* **2005**, *5*, 325−328.

(20) Zhu, H.; Zhang, H.; Liang, J.; Rao, G.; Li, J.; Liu, G.; Du, Z.; Fan, H.; Luo, J. *J. Phys. Chem. C* **2011**, *115*, 6375−6380.
(21) Li, X. L.; Cao, G. H.; Feng, C. M.; Li, Y. D. *J. Mater. Chem.* **2004**, *14*, 244−247.
(22) Mohanty, P.; Kang, T.; Kim, B.; Park, J. *J. Phys. Chem. B* **2005**, *110*, 791−795.
(23) Sen, S.; Bhatta, U. M.; Kumar, V.; Muthe, K. P.; Bhattacharya, S.; Gupta, S. K.; Yakhmi, J. V. *Cryst. Growth Des.* **2008**, *8*, 238−242.
(24) Siciliano, T.; Filippo, E.; Genga, A.; Micocci, G.; Siciliano, M.; Tepore, A. *Cryst. Res. Technol.* **2011**, *46*, 765−768.
(25) Geng, B. Y.; Lin, Y.; Peng, X. S.; Meng, G. W.; Zhang, L. D. *Nanotechnology* **2003**, *14*, 983.
(26) Martin, C. R. *Science* **1994**, *266*, 1961−1966.
(27) Adhikari, H.; McIntyre, P. C.; Marshall, A. F.; Chidsey, C. E. D. *J. Appl. Phys.* **2007**, 102.
(28) Huang, M. H.; Wu, Y.; Feick, H.; Tran, N.; Weber, E.; Yang, P. *Adv. Mater.* **2001**, *13*, 113−116.
(29) Lu, W.; Lieber, C. M. *J. Phys. D: Appl. Phys.* **2006**, *39*, R387.
(30) Wagner, R. S.; Ellis, W. C. *Appl. Phys. Lett.* **1964**, *4*, 89−90.
(31) Wu, Y.; Yang, P. *J. Am. Chem. Soc.* **2001**, *123*, 3165−3166.
(32) Wang, Z.; Wang, L.; Huang, J.; Wang, H.; Pan, L.; Wei, X. *J. Mater. Chem.* **2010**, *20*, 2457−2463.
(33) He, Z.; Yu, S.-H.; Zhu, J. *Chem. Mater.* **2005**, *17*, 2785−2788.
(34) Wang, Q.; Li, G. D.; Liu, Y. L.; Xu, S.; Wang, K. J.; Chen, J. S. *J. Phys. Chem. C* **2007**, *111*, 12926−12932.
(35) Zhu, W.; Wang, W.; Xu, H.; Zhou, L.; Zhang, L.; Shi, J. *Cryst. Growth Des.* **2006**, *6*, 2804−2808.
(36) Smith, D. L. *Thin-Film Deposition: Principles and Practice*; McGraw-Hill: New York, 1995.
(37) Mullin, J. W. *Crystallization*, 4th ed.; Butterworth-Heinemann: Oxford, U.K., 2001.
(38) Burton, W. K.; Cabrera, N.; Frank, F. C. *Philos. Trans. R. Soc., A* **1951**, *243*, 299−358.
(39) Greytak, A. B.; Lauhon, L. J.; Gudiksen, M. S.; Lieber, C. M. *Appl. Phys. Lett.* **2004**, *84*, 4176−4178.
(40) Le, S. T.; Jannaty, P.; Zaslavsky, A.; Dayeh, S. A.; Picraux, S. T. *Appl. Phys. Lett.* **2010**, *96*, No. 262102.